

Enhancing synchronization by optimal correlated noise

Sherwood Martineau,* Tim Saffold,* Timothy Chang, and Henrik Ronellenfitsch†

Physics Department, Williams College, 33 Lab Campus Drive, Williamstown, MA 01267, U.S.A.

(Dated: July 20, 2021)

From the flashes of fireflies to Josephson junctions and power infrastructure, networks of coupled phase oscillators provide a powerful framework to describe synchronization phenomena in many natural and engineered systems. Most real-world networks are under the influence of noisy, random inputs, potentially inhibiting synchronization. While noise is unavoidable, here we show that there exist optimal noise patterns which minimize desynchronizing effects and even enhance order. Specifically, using analytical arguments we show that in the case of a two-oscillator model, there exists a sharp transition from a regime where the optimal synchrony-enhancing noise is perfectly anti-correlated, to one where the optimal noise is correlated. More generally, we then use numerical optimization methods to demonstrate that there exist anti-correlated noise patterns that optimally enhance synchronization in large complex oscillator networks. Our results may have implications in real-world networks such as power grids and neuronal networks, which are subject to significant amounts of correlated input noise.

The occurrence of noise is unavoidable in networks and systems at all scales [1], from biological examples [2] such as neurons in the auditory and visual pathways [3–5], neural information processing [6, 7] to mechanical oscillators [8] and fluctuating inputs affecting the stability of power grids [9–11]. Synchronization of the underlying network of nonlinear phase oscillators is a paradigm employed to understand such physical and biological networks [12, 13]. Fluctuations are generally seen as undesirable and significant efforts have been made to understand and prevent their detrimental effects on network synchronization [14–19]. Optimization methods have been successfully employed to improve synchrony with and without noise, in particular by adjusting network weights and topology [17, 20–28]. Similar techniques have also been effective for other types of networks and objectives, such as efficient transport [29–35]. At the same time, there has been recent interest in the possibility that noise may be leveraged to enhance synchronization [36–42]. Specifically, it was found that the degree to which input noise is correlated may have a significant influence on its ability to aid in or prevent network synchrony [36].

Based on the widely used Kuramoto model [43, 44], in this work we study the optimal patterns of input noise correlations that enhance synchronization in networks of oscillators. Using analytic arguments we find that in the simple case of two coupled oscillators in the phase-drift regime as studied in Ref. [36], the optimal synchrony-enhancing noise undergoes a transition from perfect anti-correlation to perfect correlation as the total noise strength is increased. Making contact with relevant real-world networks such as power grids [9], we then numerically study generic complex networks near phase-locked fixed points and show that the optimal pattern of synchrony-enhancing noise retains the anti-correlation characteristics seen in the two-oscillator case. The optimal noise patterns we uncover are strongly linked to the underlying weighted network topology. If the topol-

ogy allows it, neighboring nodes receive perfectly anti-correlated noise. Otherwise, noise correlations decay away from each individual oscillator. In real-world complex networks, the optimal noise correlations show characteristic clustering, separating the network into regions that benefit from receiving uncorrelated inputs. We now proceed to analytically study the tractable case of two connected Kuramoto oscillators subject to generic noise.

The model consists of $N = 2$ coupled phase-oscillators with different natural frequencies. In the limit of weak coupling, the phases can be modeled using the Kuramoto-type equations

$$\begin{aligned}\frac{d\theta_1}{dt} &= \omega_1 + \frac{K}{2} \sin(\theta_2 - \theta_1) + \eta_1 \\ \frac{d\theta_2}{dt} &= \omega_2 + \frac{K}{2} \sin(\theta_1 - \theta_2) + \eta_2,\end{aligned}\quad (1)$$

where $\theta_i(t)$ are the oscillator phases, ω_i the natural frequencies, K is the coupling constant, and η_i are stochastic white noise terms satisfying $\langle \eta_i \rangle = 0$ and $\langle \eta_i(t) \eta_j(t') \rangle = C_{ij} \delta(t - t')$ with the symmetric and positive semi-definite covariance matrix $C_{ij} = C_{ji}$. The model described by Eq. (1) was recently shown to exhibit counter-intuitive enhanced synchronization under uncorrelated noise $C_{ij} \sim \delta_{ij}$ as opposed to common noise $C_{ij} = C$ [36]. We now study this effect allowing for arbitrary correlations between the noise terms. It is useful to change variables to the mean angle $\mu = (\theta_1 + \theta_2)/2$ and angular difference $\delta = \theta_1 - \theta_2$. The mean μ is irrelevant for synchronization as quantified by the squared Kuramoto order parameter $R^2 = |\sum_j e^{i\theta_j}/N|^2 = 1/2 + (1/2) \cos \delta$. We therefore focus on the dimensionless equation for the phase difference,

$$\delta'(\tau) = 1 - \kappa \sin \delta(\tau) + \zeta, \quad (2)$$

where the prime indicates a derivative with respect to $\tau = \Delta\omega t$, the dimensionless parameter $\kappa = K/\Delta\omega$, and the dimensionless noise $\zeta = (\eta_1 - \eta_2)/\Delta\omega$.

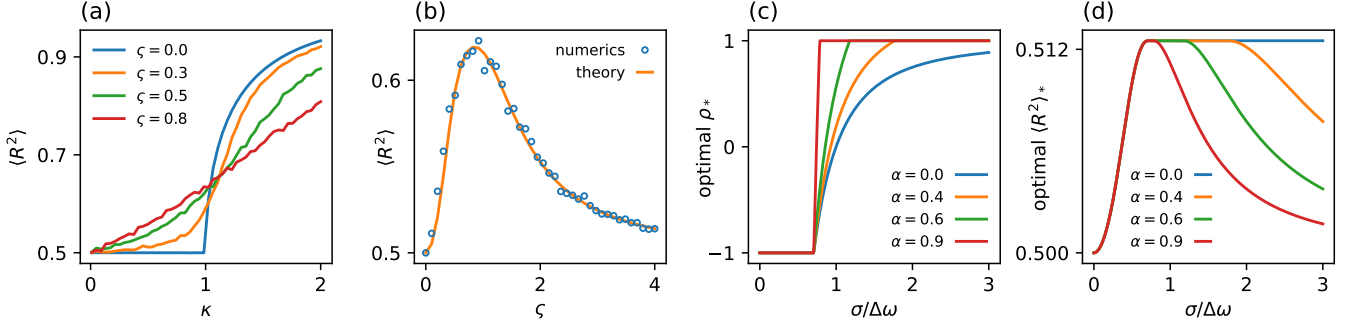


FIG. 1. Noise-enhanced synchronization in the two-oscillator model and optimal covariance transition. (a) Numerically obtained $\langle R^2 \rangle$ from integrating Eq. (2) until $\tau = 20000$ from random initial conditions as a function of $\kappa = K/\Delta\omega$ for several ζ . (b) Numerically obtained $\langle R^2 \rangle$ from integrating Eq. (2) until $\tau = 20000$ from random initial conditions (circles) and analytic approximation (see Ref. [45] for the explicit formula) as a function of ζ for $\kappa = 0.9$. (c) Approximate optimal covariance ρ_* as a function of $\sigma/\Delta\omega$ at $\kappa = 0.1$. The transition from occurs at $\sigma_c/\Delta\omega \approx 1/\sqrt{2}$. (d) Approximate optimal order parameter $\langle R^2 \rangle_*$ for the optimal covariances shown in panel (c) at $\kappa = 0.1$.

In the absence of noise, $\zeta = 0$, it is well known that Eq. (2) exhibits a synchronization phase transition at $\kappa = 1$ [43, 46]. To study the behavior with non-vanishing noise, we calculate $\langle \zeta \rangle = 0$ and

$$\begin{aligned} \langle \zeta(\tau)\zeta(\tau') \rangle &= \frac{1}{\Delta\omega^2} (C_{11} - 2C_{12} + C_{22}) \delta(\tau - \tau') \\ &= 2\zeta^2 \delta(\tau - \tau'). \end{aligned}$$

This suggests that the effective noise strength ζ^2 that is relevant for synchronization depends on the degree of correlation between the original noise inputs $\eta_{1,2}$. Specifically, for common noise, $C_{ij} = \sigma^2$ implies $\zeta^2 = 0$: Common noise does not affect synchronization at all. For uncorrelated noise, $C_{ii} = \sigma^2$ and $C_{12} = 0$, which implies $\zeta^2 = \sigma^2/(2\Delta\omega^2)$. A similar argument shows that the maximum effective noise strength for synchronization is achieved for *anti-correlated* inputs $C_{ii} = \sigma^2$, $C_{12} = -\sigma^2$ with $\zeta^2 = \sigma^2/\Delta\omega^2$.

But how does the noise strength ζ^2 affect synchronization, and can we find an optimal noise correlation? We numerically simulated Eq. (2) and computed long-time averages of the order parameter R^2 for several ζ^2 . In the regime below the transition, $\kappa < 1$, noise generally enhances synchronization, while for $\kappa > 1$, noise generally decreases synchronization {Fig. 1 (a), Ref. [36]}. At fixed κ , it becomes clear that there exists an optimal effective noise ζ_*^2 that maximizes synchronization. [Fig. 1 (b)]. Given fixed variances C_{ii} , the covariance C_{12} can be used to tune the effective noise and thus increase synchronization. We consider the general case $C_{ii} = \sigma_i^2$ and $C_{12} = \rho \sigma_1 \sigma_2$ with the correlation $-1 \leq \rho \leq 1$.

We can find an analytic approximation for the optimal effective noise strength ζ_*^2 . Equation (2) is equivalent to the Fokker-Planck equation

$$\frac{\partial p(\delta, t)}{\partial t} = -\frac{\partial}{\partial \delta} [(1 - \kappa \sin \delta) p(\delta, t)] + \zeta^2 \frac{\partial^2 p(\delta, t)}{\partial \delta^2} \quad (3)$$

for the probability density $p(\delta + 2\pi, t) = p(\delta, t)$. While Eq. (3) can not be solved exactly, in the regime of $\kappa < 1$, the steady-state distribution is approximated well by a truncated Fourier series. From the lowest order approximation, we obtain an explicit expression for $\langle R^2 \rangle(\zeta, \kappa)$ [45]. The optimal effective noise is then found to be

$$\zeta_*^2 = 1 - \frac{23}{100} \kappa^2 + \mathcal{O}(\kappa^4),$$

and the corresponding maximal order parameter is

$$\langle R^2 \rangle_* = \frac{1}{2} + \frac{\kappa}{8} + \mathcal{O}(\kappa^3).$$

In this regime, the agreement with results of full numerical solutions of the Fokker-Planck equation is excellent [Fig. 1 (b), Ref. [45]].

Expressing ζ^2 in terms of $\sigma_{1,2} = \sigma(1 \pm \alpha)$ for $\sigma = (\sigma_1 + \sigma_2)/2$, $\alpha = (\sigma_1 - \sigma_2)/(\sigma_1 + \sigma_2)$ and ρ , we find the optimal correlation to enhance synchronization as

$$\rho_* = \left[\frac{1 + \alpha^2}{1 - \alpha^2} - \frac{\Delta\omega^2}{\sigma^2} \frac{\zeta_*^2}{1 - \alpha^2} \right]_{[-1,1]},$$

where the angle brackets indicate that the argument is clipped to remain in the range $[-1, 1]$. This clipping is necessary to ensure that the matrix C parametrized in this way remains a valid covariance matrix. It also leads to a characteristic, sharp transition for the optimal correlation ρ_* , because the maximum may occur at the boundary of the allowed range [Fig. 1 (c)]. For small $\sigma/\Delta\omega$, anti-correlated noise optimally enhances synchronization. The critical noise strength σ_c above which anti-correlated noise $\rho_* = -1$ ceases to be optimal satisfies $\sigma_c/\Delta\omega = \zeta_*/\sqrt{2}$, and the critical noise strength σ_+ above which common noise $\rho_* = 1$ becomes optimal is $\sigma_+ = \sigma_c/\alpha$. In the regime where $-1 < \rho_* < 1$, the global

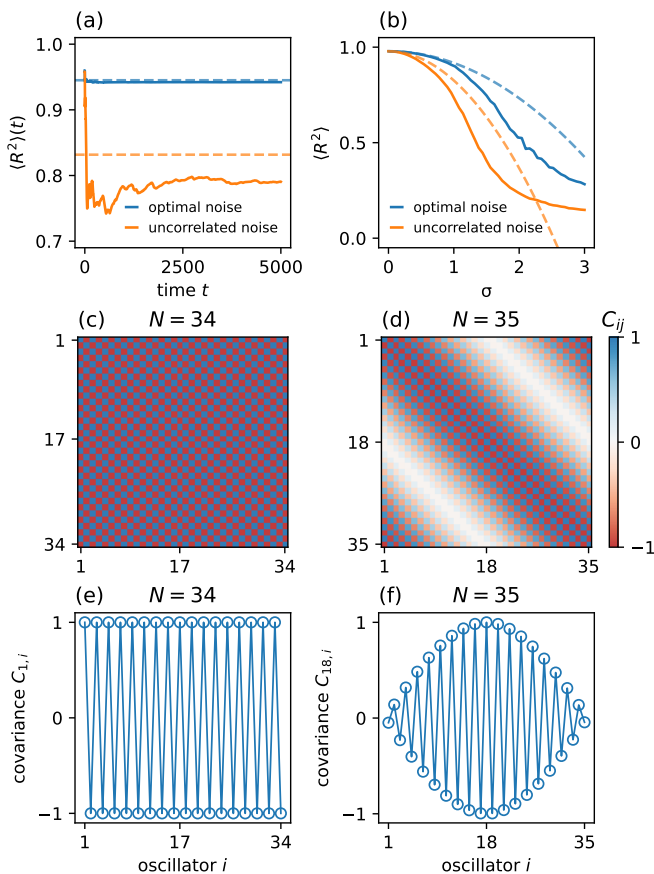


FIG. 2. Optimal noise patterns in periodic oscillator chains near fixed points. (a) Time-averaged order parameter $\langle R^2 \rangle(t) = (1/t) \int_0^t R^2(t') dt'$ in a periodic chain of $N = 34$ oscillators for optimal [panel (c)] and uncorrelated $C_{ij} = \delta_{ij} + (\delta_{ij} - 1)/(N - 1)$. Dashed lines correspond to model predictions $\langle R^2 \rangle = R_0^2 + \frac{1}{2} \text{tr}(HE)$. The noise variance $\sigma = 0.5$. (b) Numerically obtained long-time order parameters $\langle R^2 \rangle$ in a $N = 10$ periodic chain of oscillators with optimal and uncorrelated noise. Dashed lines correspond to model predictions, order parameters were obtained at $t = 15000$. (c) Optimal covariance matrix for even periodic chain of $N = 34$. (d) Optimal covariance matrix for odd periodic chain of $N = 35$. (e) Optimal covariances $C_{1,i}$ with respect to the first oscillator in the even chain. (f) Frustrated optimal covariance pattern $C_{18,i}$ with respect to the center oscillator in the odd chain. Natural frequencies in all panels were drawn from the Normal distribution $\mathcal{N}(0, 1/N^2)$, and $K = 2$.

optimum can be reached and $\langle R^2 \rangle_*$ is constant. Otherwise, while $\rho_* = \pm 1$, the optimal order parameter occurs at the boundary of the allowed range and is less than the global maximum [Fig. 1 (d)]. This general behavior remains valid for larger κ , even close to the transition $\kappa = 1$ [45].

The situation is different in the regime $\kappa > 1$ where phase-locked fixed points exist. By expanding Eq. (2) near a fixed point $\delta' = 0$, it can be shown that $\langle R^2 \rangle \approx R_0^2 - \zeta^2/4$ [45]. In this regime, common noise $\rho_* = 1$

will always optimally enhance synchronization because it minimizes ζ^2 . Unlike in the phase-drift regime, the noise-free order parameter R_0^2 can not be exceeded.

In many real-world cases such as power grids, the network operates near a phase-locked fixed point instead of in the incoherent regime. Therefore, we now focus on general networks near a fixed point and show that, unlike in the two-oscillator case, there exist optimal correlation patterns beyond common noise that enhance synchronization. The equations of motion for N oscillators are

$$\frac{d\theta_i}{dt} = \omega_i + \sum_{j=1}^N K_{ij} \sin(\theta_j - \theta_i) + \eta_i, \quad (4)$$

where again the stochastic forcing is given by correlated white noise, $\langle \eta_i(t) \eta_j(t') \rangle = C_{ij} \delta(t - t')$. The matrix $K_{ij} = K_{ji}$ encodes the weighted network topology. Equation (4) as well as the order parameter allow for the freedom to shift the phases as $\theta_i \rightarrow \theta_i - \mu$, where μ is the same for all oscillators. It is natural to consider centered dynamics where μ is the mean phase. In the following, we adopt this choice, where the mean natural frequency, the mean noise, and the mean covariance with any oscillator vanish, $\sum_i \omega_i = \sum_j \eta_j = \sum_j C_{ij} = 0$ [45]. Assuming that noise drives the centered Eq. (4) near a fixed point $0 = \omega_i + \sum_{j=1}^N K_{ij} \sin(\bar{\theta}_j - \bar{\theta}_i)$, we expand $\theta_i = \bar{\theta}_i + \varepsilon_i$ to obtain the linearized dynamics of the perturbations ε_i ,

$$\dot{\varepsilon}_i = \sum_{j=1}^N K_{ij} \cos(\bar{\theta}_j - \bar{\theta}_i) (\varepsilon_j - \varepsilon_i) + \eta_i. \quad (5)$$

We also expand the noise-averaged order parameter,

$$\langle R^2 \rangle = R_0^2 + \frac{1}{2} \langle \varepsilon^\top H \varepsilon \rangle + \mathcal{O}(\varepsilon^3), \quad (6)$$

where R_0^2 is the order parameter at the fixed point $\bar{\theta}_i$, the linear term vanished upon averaging over the noise, and we employed the Hessian matrix $H_{ij} = (2/N^2) (\cos(\bar{\theta}_i - \bar{\theta}_j) - \delta_{ij} \sum_k \cos(\bar{\theta}_i - \bar{\theta}_k))$, where δ_{ij} is the Kronecker delta. The Hessian encodes the synchronization state of the fixed point and is usually negative definite. Thus, we expect that any amount of noise will generically reduce synchrony. However, it is still possible to find noise inputs that minimize these effects. Equation (6) suggests that such optimal synchronization is achieved by maximizing the second order term $\langle \varepsilon^\top H \varepsilon \rangle = \text{tr}(HE)$. Here, $\text{tr}(\cdot)$ is the matrix trace, and $E = \langle \varepsilon \varepsilon^\top \rangle$ satisfies the continuous Lyapunov equation $LE + EL = -C$ for the weighted Laplacian matrix $L_{ij} = K_{ij} \cos(\bar{\theta}_j - \bar{\theta}_i) - \delta_{ij} \sum_n K_{in} \cos(\bar{\theta}_n - \bar{\theta}_i)$. This can be seen by formally solving Eq. (5) in the Langevin formalism and performing the noise average [45].

Our goal of finding the optimal noise covariances C can

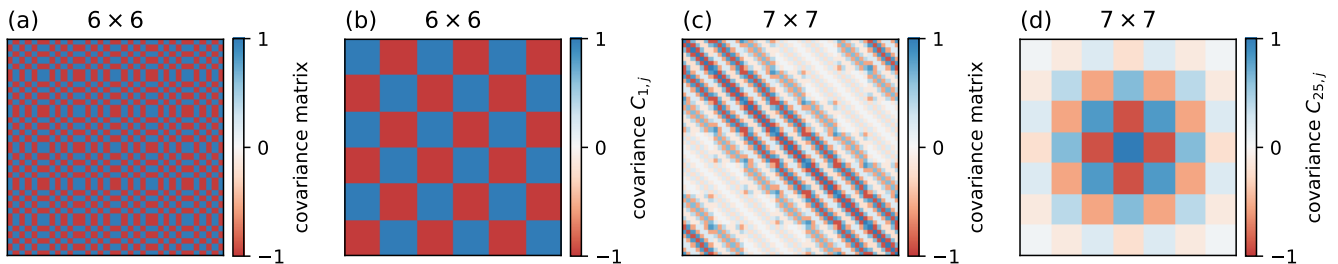


FIG. 3. Optimal noise patterns and frustrated covariances in periodic square grids. (a) Optimal covariance matrix of an unfrustrated 6×6 periodic square grid of oscillators. (b) Covariance pattern for the same grid as in panel (a) with respect to the top left oscillator, all neighbors are anti-correlated. Each matrix entry corresponds to one oscillator in the grid with neighbors as shown. (c) Optimal covariance matrix of a frustrated 7×7 periodic square grid of oscillators. Because the graph has an odd number of oscillators in each direction, not all neighbors can receive anti-correlated noise. (d) Covariance pattern for the same grid as in panel (c) with respect to the center oscillator. Covariances decay with distance, similar to Fig. 2 (d,f).

be formulated as the constrained optimization problem

$$\begin{aligned} \max_{C,E} \quad & \text{tr}(HE) \\ \text{such that} \quad & LE + EL = -C \\ & C \succeq 0. \end{aligned} \quad (7)$$

A valid covariance matrix must be positive semi-definite, $C \succeq 0$. This constraint turns the problem into a semi-definite program, for which efficient numerical algorithms are available [47]. As it stands, our optimization problem is unbounded, such that we must augment it by an additional constraint to set the noise scale. For simplicity, we consider the case of uniform variances, $C_{ii} = 1$. Because the Lyapunov equation in Eq. (7) is linear, any value C_{ii} can be obtained by rescaling the optimal solution.

To uncover the relationship between network topology and optimal noise, we numerically analyze networks of increasing complexity. For simplicity, we take the coupling constants to be uniform, $K_{ij} \equiv K/d$, where d is the network's average degree. We draw the natural frequencies from a Gaussian distribution $\omega_i \sim \mathcal{N}(0, 1/N^2)$, where N is the number of nodes. To ensure centered dynamics, the mean of the natural frequencies for each network is shifted to exactly zero. Fixed points are obtained numerically from a random initial guess, and the semi-definite program Eq. (7) is solved using the JuMP framework [48] and the COSMO algorithm [49].

As the simplest extension of our two-oscillator model we first consider periodic chains of N oscillators. We note that the optimal noise pattern obtained from solving Eq. (7) is highly effective in improving synchronization as compared to uncorrelated noise [Fig. 2 (a)], even far into the nonlinear regime [Fig. 2 (b)]. Interestingly, the optimal noise is such that neighboring pairs in chains with an even number of oscillators receive anti-correlated inputs [Fig. 2 (c,e)]. However, it is not always possible for all pairs of neighbors in a network to receive perfectly anti-correlated inputs, leading to frustrated patterns of optimal noise. Indeed, for an odd number of

oscillators in the chain, the magnitude of the optimal noise correlation $|C_{ij}|$ decays away from any particular oscillator i . The chain topology prevents any two neighboring oscillators from receiving perfectly anti-correlated noise [Fig. 2 (d,f)]. This effect is also seen in more complicated networks. In a periodic even square grid, the optimal noise is perfectly anti-correlated between neighboring nodes [Fig. 3 (a,b)], whereas for odd square grids, correlations show a characteristic decay similar to odd chains due to the fact that not all neighbors can receive perfectly anti-correlated inputs [Fig. 3 (c,d)].

Power grids are a relevant real-world complex network subject to noisy inputs. The IEEE 14-bus and 30-bus test cases [50] are power grid-derived weighted network topologies. The optimal noise patterns in these complex networks show characteristic clustering, where groups of oscillators are approximately anti-correlated among themselves. However, correlations between the clusters are approximately zero (Fig. 4). One particular type of cluster in these more realistic networks consists of one single “dangling” node which has only one neighbor, and that corresponding neighbor. Such nodes have been identified as particularly vulnerable to perturbations before [51, 52], and it is interesting that they appear to benefit from being decoupled from the rest of the network with respect to noisy inputs.

In summary, we studied to what extent synchronization in complex oscillator networks can be controlled and enhanced by correlated noise. While previous work suggested that uncorrelated noise may improve synchronization in a system of two oscillators [36], here we presented a full analysis of the effect of correlated noise. In the phase-drift regime, where noise can significantly improve synchronization, we analytically found that the optimal degree of correlation between the two noisy inputs depends strongly on the noise strength itself. For weak noise, anti-correlated inputs are optimal. Optimal noise patterns for complex networks have similar properties. We found that when the network topology permits, the

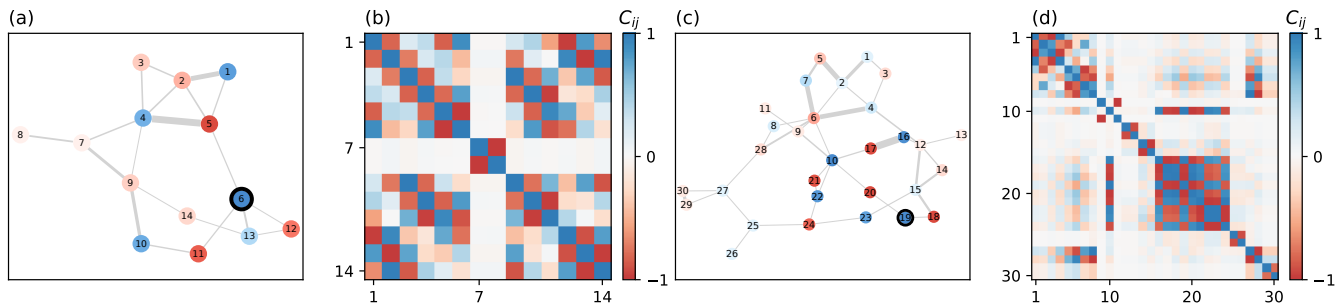


FIG. 4. Anti-correlated patterns form clusters in complex networks. (a) IEEE 14-node test grid, node colors corresponds to correlation with oscillator 6. (b) Optimal covariance matrix for the network from (a). There are two clusters of anti-correlated oscillators that are uncorrelated with each other. (c) IEEE 30-node test grid, node colors corresponds to correlation with oscillator 19. (d) Optimal covariance matrix for the network from (c). There are several clusters of anti-correlated oscillators that are uncorrelated with each other. Small clusters of two nodes generally have one of the nodes “dangling” with only one neighbor. In all graph plots, edge width is proportional to the coupling strength K_{ij} . Power loads were centered and normalized to unit variance, and then used as constant inputs.

optimal input noise is delocalized, with all neighboring nodes receiving anti-correlated input noise. Otherwise, the optimal noise is localized, with the strength of correlations decaying over a distance in the network, or even restricted to clusters of nodes.

Our results may have implications for realistic networks that operate under external noise inputs such as power grids and neuronal networks. For instance, power grid synchronization may be enhanced if new power plants and lines are judiciously placed according to the principles outlined above. Correlations of input noise can be estimated [53], or predicted from the weather [54, 55]. Thus, our work opens up new pathways to understanding and controlling synchrony in real-world complex systems.

* S.M. and T.S. contributed equally.

† hmr1@williams.edu

- [1] B. Lindner, Effects of noise in excitable systems, *Physics Reports* **392**, 321 (2004).
- [2] D. K. Wells, W. L. Kath, and A. E. Motter, Control of Stochastic and Induced Switching in Biophysical Networks, *Physical Review X* **5**, 031036 (2015).
- [3] W. Bialek, Physical Limits to Sensation and Perception, *Annual Review of Biophysics and Biophysical Chemistry* **16**, 455 (1987).
- [4] L. S. Tsimring, Noise in biology, *Reports on Progress in Physics* **77**, 026601 (2014).
- [5] J. Shlens, F. Rieke, and E. Chichilnisky, Synchronized firing in the retina, *Current Opinion in Neurobiology* **18**, 396 (2008).
- [6] H. G. Eyherabide and I. Samengo, When and Why Noise Correlations Are Important in Neural Decoding, *Journal of Neuroscience* **33**, 17921 (2013).
- [7] I. Kanitscheider, R. Coen-Cagli, and A. Pouget, Origin of information-limiting noise correlations, *Proceedings of the National Academy of Sciences* **112**, E6973 (2015).
- [8] M. H. Matheny, J. Emenheiser, W. Fon, A. Chapman, A. Salova, M. Rohden, J. Li, M. Hudoba de Badyn, M. Pósfai, L. Duenas-Osorio, M. Mesbahi, J. P. Crutchfield, M. C. Cross, R. M. D’Souza, and M. L. Roukes, Exotic states in a simple network of nanoelectromechanical oscillators, *Science* **363**, eaav7932 (2019).
- [9] P. H. Nardelli, N. Rubido, C. Wang, M. S. Baptista, C. Pomalaza-Raez, P. Cardieri, and M. Latva-aho, Models for the modern power grid, *The European Physical Journal Special Topics* **223**, 2423 (2014).
- [10] P. Milan, M. Wächter, and J. Peinke, Turbulent Character of Wind Energy, *Physical Review Letters* **110**, 138701 (2013).
- [11] B. Schäfer, C. Beck, K. Aihara, D. Witthaut, and M. Timme, Non-Gaussian power grid frequency fluctuations characterized by Lévy-stable laws and superstatistics, *Nature Energy* **3**, 119 (2018).
- [12] S. Strogatz, *Sync: How Order Emerges from Chaos In the Universe, Nature, and Daily Life* (Hachette Books, 2012).
- [13] R. E. Mirollo and S. H. Strogatz, Synchronization of Pulse-Coupled Biological Oscillators, *SIAM Journal on Applied Mathematics* **50**, 1645 (1990).
- [14] C. Luo and H. Banakar, Strategies to smooth wind power fluctuations of wind turbine generator, *IEEE Transactions on Energy Conversion* **22**, 341 (2007).
- [15] B. C. Bag, K. G. Petrosyan, and C.-K. Hu, Influence of noise on the synchronization of the stochastic Kuramoto model, *Physical Review E* **76**, 056210 (2007).
- [16] T. Yanagita and A. S. Mikhailov, Design of oscillator networks with enhanced synchronization tolerance against noise, *Physical Review E* **85**, 056206 (2012).
- [17] H. Ronellenfitsch, J. Dunkel, and M. Wilczek, Optimal Noise-Canceling Networks, *Physical Review Letters* **121**, 208301 (2018).
- [18] J. Hindes, P. Jacquod, and I. B. Schwartz, Network desynchronization by non-Gaussian fluctuations, *Physical Review E* **100**, 052314 (2019).
- [19] M. Tyloo, T. Coletta, and P. Jacquod, Robustness of Synchrony in Complex Networks and Generalized Kirchhoff Indices, *Physical Review Letters* **120**, 084101 (2018).
- [20] M. Fazlyab, F. Dörfler, and V. M. Preciado, Optimal network design for synchronization of coupled oscillators,

- Automatica* **84**, 181 (2017).
- [21] T. Tanaka and T. Aoyagi, Optimal weighted networks of phase oscillators for synchronization, *Physical Review E* **78**, 046210 (2008).
- [22] M. Brede, Synchrony-optimized networks of non-identical Kuramoto oscillators, *Physics Letters A* **372**, 2618 (2008).
- [23] B. Li and K. Y. M. Wong, Optimizing synchronization stability of the Kuramoto model in complex networks and power grids, *Physical Review E* **95**, 012207 (2017).
- [24] D. Kelly and G. A. Gottwald, On the topology of synchrony optimized networks of a Kuramoto-model with non-identical oscillators, *Chaos: An Interdisciplinary Journal of Nonlinear Science* **21**, 025110 (2011).
- [25] M. Fardad, F. Lin, and M. R. Jovanovic, Design of Optimal Sparse Interconnection Graphs for Synchronization of Oscillator Networks, *IEEE Transactions on Automatic Control* **59**, 2457 (2014).
- [26] P. S. Skardal, D. Taylor, and J. Sun, Optimal synchronization of complex networks, *Physical Review Letters* **113**, 1 (2014).
- [27] F. Dörfler and F. Bullo, Synchronization and Transient Stability in Power Networks and Nonuniform Kuramoto Oscillators, *SIAM Journal on Control and Optimization* **50**, 1616 (2012).
- [28] M. Alhazmi, P. Dehghanian, S. Wang, and B. Shinde, Power Grid Optimal Topology Control Considering Correlations of System Uncertainties, *IEEE Transactions on Industry Applications* **55**, 5594 (2019).
- [29] M. Durand, Structure of Optimal Transport Networks Subject to a Global Constraint, *Physical Review Letters* **98**, 088701 (2007).
- [30] S. Bohn and M. O. Magnasco, Structure, Scaling, and Phase Transition in the Optimal Transport Network, *Physical Review Letters* **98**, 088702 (2007).
- [31] E. Katifori, G. J. Szöllösi, and M. O. Magnasco, Damage and Fluctuations Induce Loops in Optimal Transport Networks, *Physical Review Letters* **104**, 048704 (2010).
- [32] J. W. Rocks, H. Ronellenfitch, A. J. Liu, S. R. Nagel, and E. Katifori, Limits of multifunctionality in tunable networks, *Proceedings of the National Academy of Sciences* **116**, 2506 (2019).
- [33] J. B. Kirkegaard and K. Sneppen, Optimal Transport Flows for Distributed Production Networks, *Physical Review Letters* **124**, 208101 (2020).
- [34] F. Kaiser, H. Ronellenfitch, and D. Witthaut, Discontinuous transition to loop formation in optimal supply networks, *Nature Communications* **11**, 5796 (2020).
- [35] H. Ronellenfitch, Optimal Elasticity of Biological Networks, *Physical Review Letters* **126**, 038101 (2021).
- [36] Z. G. Nicolaou, M. Sebek, I. Z. Kiss, and A. E. Motter, Coherent Dynamics Enhanced by Uncorrelated Noise, *Physical Review Letters* **125**, 094101 (2020).
- [37] J. H. Meng and H. Riecke, Synchronization by uncorrelated noise: interacting rhythms in interconnected oscillator networks, *Scientific Reports* **8**, 6949 (2018).
- [38] K. H. Nagai and H. Kori, Noise-induced synchronization of a large population of globally coupled nonidentical oscillators, *Physical Review E* **81**, 065202 (2010).
- [39] H. Nakao, K. Arai, and Y. Kawamura, Noise-Induced Synchronization and Clustering in Ensembles of Uncoupled Limit-Cycle Oscillators, *Physical Review Letters* **98**, 184101 (2007).
- [40] C. Zhou, J. Kurths, I. Z. Kiss, and J. L. Hudson, Noise-Enhanced Phase Synchronization of Chaotic Oscillators, *Physical Review Letters* **89**, 014101 (2002).
- [41] H. Nakao, Phase reduction approach to synchronisation of nonlinear oscillators, *Contemporary Physics* **57**, 188 (2016).
- [42] M. Aravind, S. Sinha, and P. Parmananda, Competitive interplay of repulsive coupling and cross-correlated noises in bistable systems, *Chaos: An Interdisciplinary Journal of Nonlinear Science* **31**, 061106 (2021).
- [43] Y. Kuramoto, *Chemical Oscillations, Waves, and Turbulence*, Springer Series in Synergetics, Vol. 19 (Springer, Berlin, Heidelberg, 1984).
- [44] J. A. Acebrón, L. L. Bonilla, C. J. Pérez Vicente, F. Ritort, and R. Spigler, The Kuramoto model: A simple paradigm for synchronization phenomena, *Reviews of Modern Physics* **77**, 137 (2005).
- [45] Supplemental Material.
- [46] F. Dörfler and F. Bullo, On the Critical Coupling for Kuramoto Oscillators, *SIAM Journal on Applied Dynamical Systems* **10**, 1070 (2011).
- [47] L. Vandenberghe and S. Boyd, Semidefinite Programming, *SIAM Review* **38**, 49 (1996).
- [48] I. Dunning, J. Huchette, and M. Lubin, JuMP: A modeling language for mathematical optimization, *SIAM Review* **59**, 295 (2017).
- [49] M. Garstka, M. Cannon, and P. Goulart, COSMO: A conic operator splitting method for large convex problems, in *European Control Conference* (2019) arXiv:1901.10887.
- [50] University of Washington, [Power systems test case archive](#).
- [51] M. Tyloo, L. Pagnier, and P. Jacquod, The key player problem in complex oscillator networks and electric power grids: Resistance centralities identify local vulnerabilities, *Science Advances* **5**, eaaw8359 (2019).
- [52] D. Manik, M. Rohden, H. Ronellenfitch, X. Zhang, S. Hallerberg, D. Witthaut, and M. Timme, Network susceptibilities: Theory and applications, *Physical Review E* **95**, 012319 (2017).
- [53] L. Zhu and J. Lin, Learning Spatiotemporal Correlations for Missing Noisy PMU Data Correction in Smart Grid, *IEEE Internet of Things Journal* **8**, 7589 (2021).
- [54] P. E. Bett and H. E. Thornton, The climatological relationships between wind and solar energy supply in Britain, *Renewable Energy* **87**, 96 (2016).
- [55] K. van der Wiel, H. C. Bloomfield, R. W. Lee, L. P. Stoop, R. Blackport, J. A. Screen, and F. M. Selten, The influence of weather regimes on European renewable energy production and demand, *Environmental Research Letters* **14**, 094010 (2019).

SUPPLEMENTAL MATERIAL

APPROXIMATE SOLUTION OF THE FOKKER-PLANCK EQUATION

While Eq. (3) can not be solved analytically, in the regime of $\kappa \ll 1$, the steady-state distribution appears to be well-represented by sinusoids. Encouraged by this, we approximate the steady-state distribution as a truncated Fourier series, $p(\delta) \approx \sum_{k=-N}^N a_k e^{ik\delta}$. The normalization condition $\int_{-\pi}^{\pi} p(\delta) d\delta = 1$ implies $a_0 = 1/(2\pi)$ and reality of the solution is equivalent to $a_{-k} = a_k^*$. Plugging in the shortest non-trivial Fourier series with $N = 2$ and solving the resulting system of equations using Mathematica software yields an excellent approximation to the expected order parameter as

$$\begin{aligned} \langle R^2 \rangle &= \frac{1}{2} + \frac{1}{2} \langle \cos \delta \rangle = \frac{1}{2} + \frac{\pi}{2} (a_1 + a_1^*) \\ &= \frac{1}{2} + \frac{2\kappa\zeta^2 (\kappa^2 + 8\zeta^4 + 2)}{(\kappa^2 - 4)^2 + 16(\kappa^2 + 5)\zeta^4 + 64\zeta^8} \end{aligned} \quad (\text{S1})$$

where the expectation value is defined as $\langle f(\delta) \rangle = \int_{-\pi}^{\pi} f(\delta) p(\delta) d\delta$. This equation can be optimized directly with respect to ζ by setting the derivative to zero and solving in Mathematica.

The first approximation found above can be compared to numerical solutions. Specifically, we are interested in the optimal effective noise strength ζ_*^2 and the corresponding optimal order parameter $\langle R^2 \rangle_*$. We solved the Fokker-Planck equation Eq. (3) numerically using Mathematica and numerically obtained ζ_*^2 and $\langle R^2 \rangle_*$ using a Golden Section search (termination accuracy was set to 10^{-6}) as a function of κ . Except for values of κ close to 1, the approximation formulas are very good (Fig. S1).

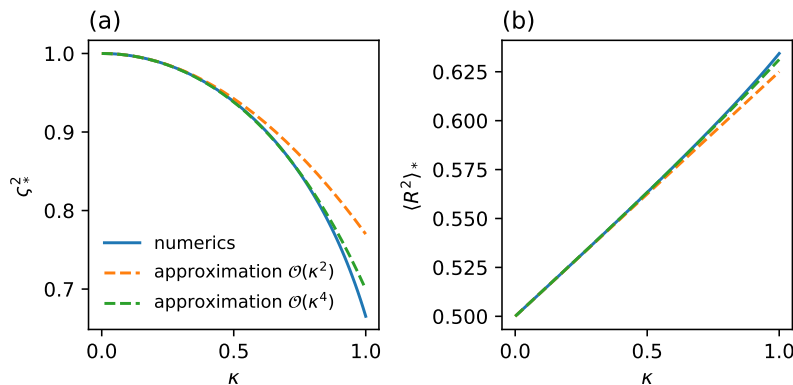


FIG. S1. Comparison of the approximation formulas derived in the main text to corresponding numerically obtained optimal values from a full numerical solution of the Fokker-Planck equation Eq. (3). (a) Optimal effective noise strength where the approximation formula is $\zeta_*^2 \approx 1 - 23\kappa^2/100 - 1757\kappa^4/25000$. Note that in the main paper, only the expression to order $\mathcal{O}(\kappa^2)$ is given. (b) Optimal order parameter where the approximation formula is $\langle R^2 \rangle_* \approx 1/2 + \kappa/8 + \kappa^3/160$. Note that in the main paper, only the expression to order $\mathcal{O}(\kappa)$ is given. The colored lines have the same interpretation as in panel (a).

TWO-OSCILLATOR MODEL NEAR A FIXED POINT

Here, we analyze the two-oscillator model near a fixed point. We start by computing the fixed point in the noise-free case,

$$\delta' = 0 \Rightarrow \bar{\delta} = \arcsin(\kappa^{-1}).$$

We now expand the equation of motion with noise close to the fixed point, $\delta(\tau) = \bar{\delta} + \varepsilon(\tau)$ as

$$\begin{aligned} \delta' = \varepsilon' &= 1 - \kappa \sin(\bar{\delta} + \varepsilon) + \zeta \\ &\approx -\sqrt{1 - \kappa^{-2}} \varepsilon + \zeta. \end{aligned} \quad (\text{S2})$$

We can similarly expand the order parameter,

$$\begin{aligned} R^2 &= \frac{1}{2} + \frac{1}{2} \cos(\bar{\delta} + \varepsilon) \\ &= R_0^2 - \frac{1}{2\kappa} \varepsilon - \frac{1}{4} \sqrt{1 - \kappa^{-2}} \varepsilon^2 + \mathcal{O}(\varepsilon^3), \end{aligned} \quad (\text{S3})$$

where $R_0^2 = (1/2)(1 + \sqrt{1 - \kappa^{-2}})$. Averaging Eq. (S3) over the noise, the term linear in ε drops out and we are left with

$$\langle R^2 \rangle = R_0^2 - \frac{1}{4} \sqrt{1 - \kappa^{-2}} \langle \varepsilon^2 \rangle.$$

To calculate the average $\langle \varepsilon^2 \rangle$, we formally solve Eq. (S2) as

$$\varepsilon(\tau) = \varepsilon_0 e^{-\sqrt{1 - \kappa^{-2}}\tau} + e^{-\sqrt{1 - \kappa^{-2}}\tau} \int_0^\tau ds e^{\sqrt{1 - \kappa^{-2}}s} \zeta(s).$$

For long times, the first term vanishes and we can use the second term to calculate

$$\begin{aligned} \langle \varepsilon(\tau)^2 \rangle &= e^{-2\sqrt{1 - \kappa^{-2}}\tau} \int_0^\tau ds \int_0^\tau ds' \langle \zeta(s)\zeta(s') \rangle e^{\sqrt{1 - \kappa^{-2}}(s+s')} \\ &= \int_0^\tau dy \int_0^\tau dy' \langle \zeta(\tau - y)\zeta(\tau - y') \rangle e^{-\sqrt{1 - \kappa^{-2}}(y+y')}, \\ &= 2\zeta^2 \int_0^\tau dy \int_0^\tau dy' \delta(y' - y) e^{-\sqrt{1 - \kappa^{-2}}(y+y')}, \end{aligned}$$

where we substituted $y = \tau - s$, $y' = \tau - s'$. Taking the limit $\tau \rightarrow \infty$, we end up with

$$\langle \varepsilon^2 \rangle = 2\zeta^2 \int_0^\infty dy e^{-2\sqrt{1 - \kappa^{-2}}y} = \frac{\zeta^2}{\sqrt{1 - \kappa^{-2}}}.$$

Plugging this expression back into Eq. (S3), we obtain

$$\langle R^2 \rangle = R_0^2 - \frac{1}{4} \zeta^2.$$

CENTERED DYNAMICS OF COMPLEX NETWORKS

Eq. (4) from the main paper contains a freedom of re-defining $\theta_i \rightarrow \theta_i + c$ for some constant c corresponding to a reference angle. Here, we fix this freedom by introducing the new variables

$$\begin{aligned} \delta_i(t) &= \theta_i(t) - \mu(t) \\ \mu(t) &= \frac{1}{N} \sum_j \theta_j(t). \end{aligned}$$

Taking derivatives and plugging them into Eq. (1), we find that they satisfy

$$\dot{\delta}_i = \omega_i - \frac{1}{N} \sum_j \omega_j(t) + \sum_j K_{ij} \sin(\delta_i - \delta_j) + \eta_i - \frac{1}{N} \sum_j \eta_j(t) \quad (\text{S4})$$

$$\dot{\mu} = \frac{1}{N} \sum_j \omega_j(t) + \frac{1}{N} \sum_j \eta_j(t), \quad (\text{S5})$$

where we used $\sum_{i,j} K_{ij} \sin(\delta_i - \delta_j) = 0$ due to antisymmetry. Equation (S4) is equivalent to Eq. (4) but with centered inputs, $\omega_i \rightarrow \omega_i - (1/N) \sum_j \omega_j(t)$ and $\eta_i \rightarrow \eta_i - (1/N) \sum_j \eta_j(t)$. The order parameter R^2 is independent of μ , so it is sufficient to consider centered dynamics and assume that $\sum_j \omega_j = 0$. However, we must consider the effect of

centering on the stochastic inputs. Specifically, the centered noisy inputs can be written using a projection matrix Q as

$$Q\boldsymbol{\eta} = \left(\mathbf{1} - \frac{1}{N}J \right) \boldsymbol{\eta},$$

where $J_{ij} = 1$. Similarly, if $\langle \eta_i(t)\eta_j(t') \rangle = C_{ij}\delta(t-t')$, then the centered correlation matrix is

$$Q\langle \boldsymbol{\eta}(t)\boldsymbol{\eta}^\top(t') \rangle Q^\top = QCQ\delta(t-t'). \quad (\text{S6})$$

Thus, the centered covariances are constrained to have vanishing row and column sums, $\sum_j C_{ij} = \sum_i C_{ij} = 0$. This is also automatically enforced by the Lyapunov equation constraint in Eq. (7).

DERIVATION OF THE LYAPUNOV EQUATION CONSTRAINT

Here, we compute the variance of fluctuations directly in the Langevin formalism. We consider the linearized second-order system from the main paper,

$$\dot{\boldsymbol{\varepsilon}} = L\boldsymbol{\varepsilon} + \boldsymbol{\eta}(t),$$

where $\langle \boldsymbol{\eta} \rangle = \mathbf{0}$, $\langle \boldsymbol{\eta}(t)\boldsymbol{\eta}^\top(t') \rangle = C\delta(t-t')$ is white noise input in time with centered correlation matrix C and L is the weighted graph Laplacian with components $L_{ij} = K_{ij}\cos(\bar{\theta}_j - \bar{\theta}_i) - \delta_{ij}\sum_n K_{in}\cos(\bar{\theta}_n - \bar{\theta}_i)$. The solution to this system can be expressed as

$$\boldsymbol{\varepsilon}(t) = \exp(Lt)\boldsymbol{\varepsilon}_0 + \int_0^t \exp(L(t-s))\boldsymbol{\eta}(s) ds.$$

The homogeneous solution $\exp(-Lt)\boldsymbol{\varepsilon}_0$ decays for large times except for a constant angular shift. In the centered dynamics, this shift vanishes and we can focus on the particular solution.

We want to compute the matrix of correlations for long times,

$$\begin{aligned} \langle \boldsymbol{\varepsilon}(t)\boldsymbol{\varepsilon}(t)^\top \rangle &= \int_0^t ds \int_0^t ds' \exp(L(t-s))\langle \boldsymbol{\eta}(s)\boldsymbol{\eta}(s')^\top \rangle \exp(L(t-s')) \\ &= \int_0^t ds \int_0^t ds' \exp(L(t-s))C\exp(L(t-s'))\delta(s-s') \\ &= \int_0^t dy \int_0^t dy' \exp(Ly)C\exp(Ly')\delta(y'-y) \end{aligned} \quad (\text{S7})$$

We substituted $y = t - s, y' = t - s'$, and used the fact that $\langle \boldsymbol{\eta}(t)\boldsymbol{\eta}^\top(t') \rangle = C\delta(t-t')$. Since we want to find the equal-time covariance in the long-time limit, we now take the limit $t \rightarrow \infty$. Integrating over the δ -function we obtain

$$\langle \boldsymbol{\varepsilon}\boldsymbol{\varepsilon}^\top \rangle = \int_0^\infty dy \exp(Ly)C\exp(Ly)$$

This matrix-valued integral cannot be evaluated directly, but we can integrate by parts to obtain

$$\begin{aligned} \langle \boldsymbol{\varepsilon}\boldsymbol{\varepsilon}^\top \rangle &= E = \int_0^\infty dy \exp(Ly)C\exp(Ly) \\ &= [\exp(Ly)C\exp(Ly)]_0^\infty L^\dagger - L \int_0^\infty dy \exp(Ly)C\exp(Ly)L^\dagger \\ &= -CL^\dagger - LEL^\dagger \\ \Rightarrow LE + EL &= -C. \end{aligned} \quad (\text{S8})$$

Here, the dagger represents the Moore-Penrose pseudo-inverse, which is used because the nullspace of L and C is given by the vector $\mathbf{1}$ of all ones. The solution E must also have $E\mathbf{1} = 0$ in the centered frame, such that Eq. (S8) captures it fully.

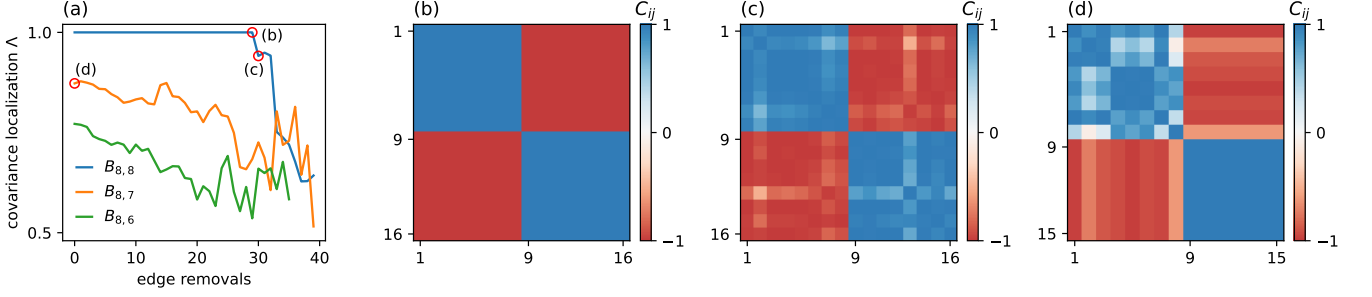


FIG. S2. Localization of optimal covariances in bipartite graphs. (a) Localization Λ of the optimal covariance matrix as edges are randomly removed from the complete bipartite graphs $B_{8,8}$, $B_{8,7}$, $B_{8,6}$. The red circles correspond to the optimal covariance matrices shown in panels (b–d). The matrices (b) and (d) change discontinuously over a single removed edge that lead to one node having only a single neighbor. In panels (b–d) the matrices C_{ij} are ordered such that for the bipartite graph $B_{n,m}$, the two sets of n and m nodes follow each other. For all optimizations, the initial fixed point was obtained at $K = 2$. Natural frequencies ω_i were chosen at random for each graph and remained unchanged as edges were removed.

LOCALIZATION OF OPTIMAL COVARIANCE IN BIPARTITE GRAPHS

Our results suggest that bipartite graphs $B_{n,m}$, where the set of $n + m$ nodes can be partitioned into two subsets of n and m nodes each and edges only connect nodes in different subsets, may form a good model for networks that can receive non-local anti-correlated noise. The degree to which the covariance matrix shows delocalization can be quantified using the measure

$$\Lambda = \frac{1}{N^2} \sum_{i,j} |C_{ij}|,$$

where N is the total number of nodes in the network. Non-local noise inputs lead to $\Lambda = 1$, and any degree of localization decreases the value of Λ . Balanced complete bipartite graphs $B_{n,n}$ generically lead to optimal noise patterns that are perfectly anti-correlated between the two groups of nodes [Fig. S2 (b)]. However, being balanced and bipartite is not sufficient for such an optimal noise pattern. This can be seen by randomly removing edges, starting from the complete graph $B_{n,n}$. Removing edges does not change the properties of being balanced and bipartite, but does change the specific network topology. Generically, there exists a transition beyond which the network connectivity no longer supports delocalized optimal noise [Fig. S2 (a–c)]. Unbalanced bipartite graphs generally do not feature perfectly anti-correlated optimal noise patterns, even when they are complete [Fig. S2 (a,d)]. In all cases of bipartite graphs we study, the degree of delocalization generally tends to decrease as edges are removed randomly [Fig. S2 (a)].